On the structures and quantification of recurrence plots

Jianbo Gao [a, *], Huaqing Cai [b]

[a] *Department of Electrical Engineering, University of California, Los Angeles, Los Angeles, CA 90095, USA*
[b] *Department of Atmospheric Sciences, University of California, Los Angeles, Los Angeles, CA 90095, USA*

Abstract

Recurrence plots (RPs) often have fascinating structures, especially when the embedding dimension is 1. We identify four basic patterns of a RP, namely, patterns along the main (45°) diagonal, patterns along the 135° diagonal, block-like structures, and square-like textures. We also study how the structures of and quantification statistics for RPs vary with the embedding parameters. By considering the distribution of the main diagonal line segments for chaotic systems, we relate some of the known statistics for the quantification of a RP to the Lyapunov exponent. This consideration enables us to introduce new ways of quantifying the diagonal line segments. Furthermore, we categorize recurrence points into two classes. A number of new quantities are identified which may be useful for the detection of nonstationarity in a time series, especially for the detection of a bifurcation sequence. A noisy transient Lorenz system is studied, to demonstrate how to identify a true bifurcation sequence, to interpret false bifurcation points, and to choose the embedding dimension. © 2000 Published by Elsevier Science B.V. All rights reserved.

1. Introduction

Recurrence plots (RPs) were initially designed to graphically display recurring patterns and nonstationarity in time series [1]. Recurring patterns are among the most important features of chaotic systems, while nonstationarity may arise from a variety of reasons such as drifting of a parameter, time-varying nature of a driving force, sudden changes in dynamics, etc. It is thus no wonder that ever since RPs were introduced, RPs have found utility in a wide range of scientific explorations. For instance, RPs have been used to study various biological systems including neuronal spike trains [2], quiet and active breathing [3], electromyographic (EMG) data [4], periodically modulated inhibition [5], mood variation in bipolar disorder [6], synaptic noise of a central neuron [7], intracranial EEG recordings [8], rhythmic eye movements [9], older-age tachogram data [10], and protein sequence [11;12] and dynamics [13]. A number of statistics have also been proposed to quantify RPs [3;14].

One of the major reasons that RPs are popular lies in the fact that the structures of RPs are visually appealing. See, for instance, some RPs in Iwanski and Bradley [15] (see also Fig. 2). To promote further applications of RPs in the analysis of nonlin-

---

* Corresponding author; Some source Fortran codes can be obtained through gjb@ucla.edu.
E-mail address: gjb@ucla.edu (J. Gao).

ear time series arising from diverse disciplines of science, it would be very desirable that the basic structures of RPs can be understood geometrically. As mentioned earlier, one of the initial purposes of RPs is to show recurrent patterns in chaotic systems, while the time-delay embedding technique [16;17] has long become a starting point for the analysis of chaotic time series, one naturally expects that the structures of RPs will generally depend on the embedding parameters, especially the embedding dimension. However, Iwanski and Bradley [15] claim that the structures of RPs for the many low-dimensional systems they have studied do not depend on the embedding dimension very much. In particular, they claim that in detecting bifurcations using the statistics introduced in [3;14], embedding need not be done. Understanding qualitatively the structures of RPs, how the structures of and the quantification statistics for RPs depend upon the embedding parameters will thus constitute the first goal of this Letter.

The quantification statistics for RPs introduced in [3;14], though interesting, have not been carefully studied to be related to the invariants of a chaotic system such as the Lyapunov exponents, dimension or entropy, when a chaotic time series is studied via RPs. We shall make efforts to relate some of the statistics of [3;14] to the Lyapunov exponents of a chaotic system. We will also show in this Letter that the recurrence points constituting a RP can be further classified as true recurrence points and sojourn points. This classification allows us to introduce new ways of quantifying RPs.

One of the more interesting applications of RPs to the study of an experimental time series is its ability to detect a bifurcation sequence [14;15]. In an exploratory scientific study, the underlying bifurcation sequence is, however, unknown. Hence, it is equally or even more important that that quantity may not suggest false bifurcations. And if it does, that quantity itself should suggest a way to allow one to interpret the latter. One should also bear in mind that an experimental time series is typically noise corrupted. To understand the effects of noise on an algorithm for the detection of a bifurcation sequence is thus of great practical value. The final purpose of this Letter is to show how one may make efforts to identify the true bifurcation sequence and the causes for the false bifurcation points, and to show how one

may choose suitable embedding parameters so that the algorithm may still work when the signal is heavily noise corrupted.

2. Structures of recurrence plots and their quantifications

Given a scalar time series $\{x(i), i = 1,2,\ldots\}$, it is now customary to form vectors of the form [16;17]: $X_i = (x(i), x(i + L), \ldots, x(i + (m - 1)L))$, with m being the embedding dimension and L the delay time. $\{X_i, i = 1,2, \cdots, N\}$ then represents certain trajectory in a m-dimensional space. RPs are $N \times N$ arrays in which a dot is placed at (i, j) whenever a point X_i on the trajectory is close to another point X_j. In its original form, the closeness between X_i and X_j is simply expressed by $\|X_i - X_j\| \le d$, where the scale d is a prescribed number. One may modify the definition for closeness by requiring $d_1 \le \|X_i - X_j\| \le d_2$. When d (or d_1 and d_2) is dependent upon location in the time series or in the phase space, the constructed RP can be slightly asymmetric about the main (45°) diagonal. Such a version was originally used by Eckmann et al. [1]. However, we shall simply fix d (or d_1 and d_2) so that the RP is symmetric about the main diagonal. An example is shown in Fig. 1 for a sine wave signal, $x(t) = \sin(2\pi t)$, where we used $m = 1$ and $d = 2^{-4}$. Since our Rps are symmetric, to save space in the following discussions, we shall only plot half of the RP (i.e., at the upper left or lower right triangular part).

We shall adopt Euclidean norm in our numerical simulations. However, our analysis and geometrical arguments apply to any form of norms. We note that $(0,d)$ simply represents a ball centered around X_i or X_j. (d_1,d_2) is called a corridor in [15], and a shell in [18–20]. When $d_1 = 0$, then the modified version reduces to the original form. The introduction of shells is purported at capturing the concept of scales in dynamical systems, which is so important in the study of the effects of dynamic noise on chaotic systems [21–24]. While one may still want to use the concept of shells to combat the notorious effects of noise on some statistics of RPs, we will argue below that the concept of a shell makes the interpretation and computation of certain statistics for RPs much harder.
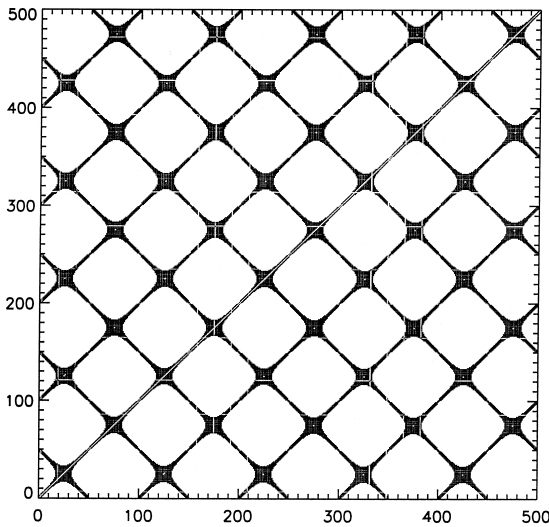
Fig. 1. A 'full' RP generated from sine wave.

Figs. 2(A,B), (C,D) and (E,F) show respectively the RPs for time series generated from (i) sine wave; (ii) quasi-periodic signal (torus), $x(t) = \sin(2\pi t) + \sin(2\sqrt{2}\,\pi t)$; and (iii) the x-component of the chaotic Lorenz system [25],

$$dx/dt = -10(x - y), \quad dy/dt = -xz + rx - y,$$
$$dz/dt = xy - 8z/3. \tag{1}$$

with the parameter r being 28. The sampling time for all three systems is 0.01. Each time series is first normalized to the unit interval $(0,1)$ before analysis. Each figure actually contains two RPs, located at the upper left and lower right triangular parts, respectively. For ease of explaining the parameters used to obtain each RP, we shall further denote each RP by 1 and 2, such as A1 and A2 for the upper left and lower right triangular parts, etc. The embedding parameters used are then $m = 1$ for (A,C,E), $m = 2$ for (B,D1,F1), $m = 3$ for (D2,F2), $L = 25, 15, 25$ for (B,D,F). The shells (or balls) used to define the RPs are $(2^{-9/2}, 2^{-4})$ for (A1,C1,E1), $(2^{-5}, 2^{-9/2})$ for (A2), $(2^{-5/2}, 2^{-2})$ for (B1,D), $(2^{-7/2}, 2^{-3})$ for (B2), $(2^{-13/2}, 2^{-6})$ for (C2,E2), and $(0, 2^{-4})$ for (F).

First we observe the dependence of RPs on the embedding dimension m. The structures of RPs for $m = 1$ are very different from those for $m = 2$ and 3, while those for $m = 2$ are quite similar to those for $m = 3$. The similarity is due to the low-dimensionality and smallness of the data set (i.e., a few hundred points) used to compute those RPs. The difference is due to false recurrences, as will be explained shortly. We also note that Figs. 2(A1,E) are quite similar to those of [15]. Thus, we are quite puzzled by the fact that this dependence of RPs on the embedding dimension m was not observed by Iwanski and Bradley [15].

Next we observe that RPs computed based on different shells are also different, especially when the embedding dimension is 1. This dependence was also observed by Iwanski and Bradley [15]. However, this dependence can be fairly easily explained. Suppose one is to fold the lower right RPs of Figs. 2(A-E) onto the upper left RPs, then one will observe that the lines of the resulting plots just become thicker. This point should be easy to understand if one performs such a procedure on Fig. 2(A), then compares the result with Fig. 1. In fact, when a ball is used instead of a shell to compute a RP, then one only observes thick solid lines (Fig. 1 and Fig. 2(F)). Put in another way, if one partitions a ball into a series of shells, then the RP corresponding to the ball splits into a series of RPs corresponding to different shells. This splitting sometimes breaks a continuous structure such as a continuous line. This may complicate computation of some statistics for RPs (for example, if that statistic is based on the length of certain line segments. See below for more details).

Since the structures of RPs for $m = 1$ are far richer and fascinating, we shall basically focus on explaining how those structures are formed. In the process of this explanation, of course, the structures of RPs for $m > 1$ will automatically become clear. For this purpose, we first note that the structures of RPs for $m = 1$ consist of four distinct features: (i) Patterns along the main (45°) diagonal. These correspond to when X_i and X_j are close, then X_{i+k} and X_{j+k} are also close together for a series of k's. (ii) Patterns along the 135° diagonal. These correspond to when X_i and X_j are close, then X_{i+k} and X_{j-k} are also close together for a series of k's. (iii) The blocks corresponding to the crossings of the above two patterns. (iv) Short vertical and horizontal lines. These are the sojourn points, as will be explained in Section 4. These sojourn points, combined with Patterns (i)–(iii), make the appearance of RPs wavy.
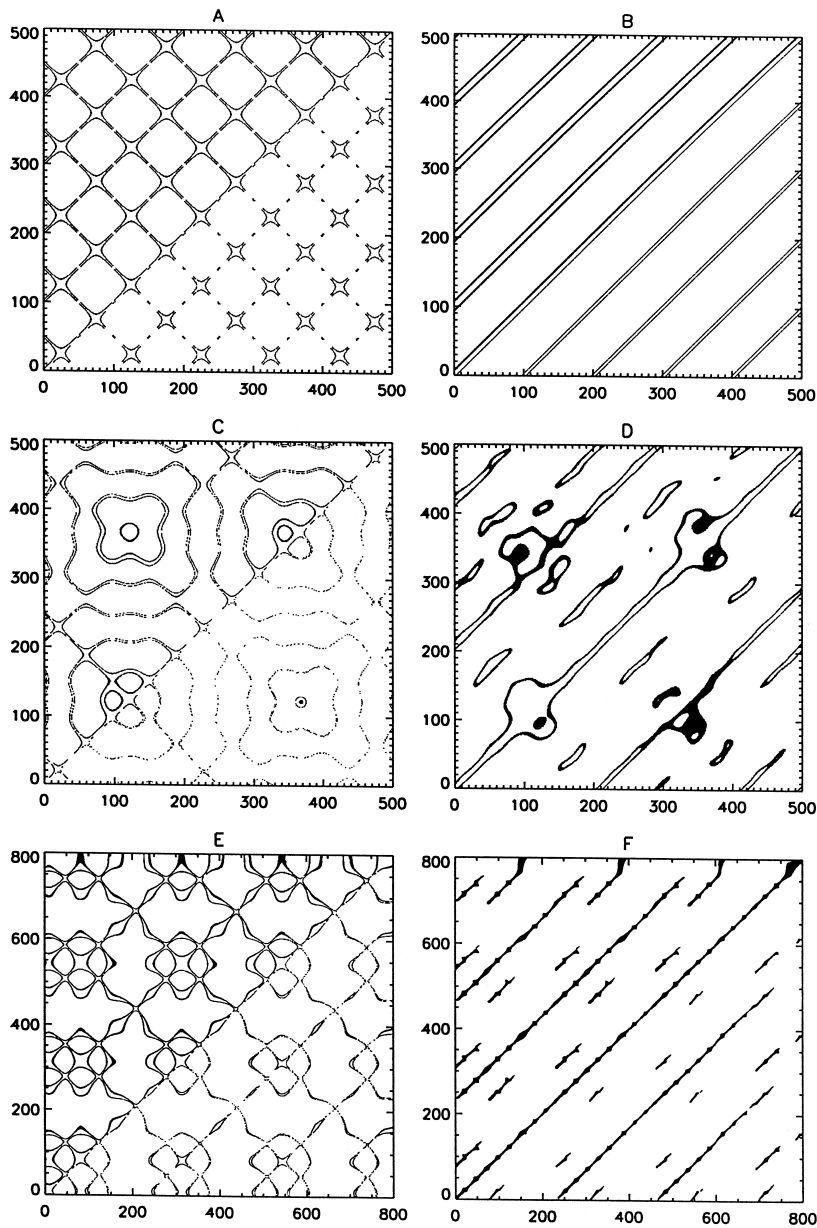
Fig. 2. 'Half' RPs generated from (i) sine wave, (ii) torus, and (iii) Lorenz system. See the text for the details.

There are two different mechanisms for the formation of the Patterns (i). One mechanism is that when two points on the same orbit keep close together for quite a while, such as pairs of points (A1, A2), (B2, B1), (C1,C2), and (D2,D1), as schematically shown in Figs. 3(a,b). Such closeness is termed autocorrelation by Theiler [26], and tangential motion by Gao and Zheng [18–20]. The term autocorrelation emphasizes averaging effect, while tangential motion emphasizes locality and motion. However,
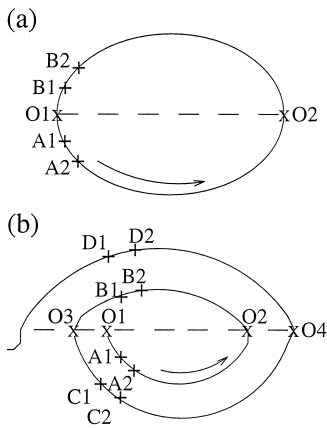
(a)

(b)

Fig. 3. A schematic explaining how a RP is composed. The direction of motion is assumed to be counterclockwise.

one needs to realize that spatial closeness does not necessarily mean temporal closeness. Another mechanism is that pairs of points on different orbits keep close together for quite a while, such as pairs of points (A1,C1), (A2,C2), (D2,B2), and (B1,D1) in Fig. 3(b). For chaotic systems, such closeness breaks down exponentially fast. Hence, the length of main diagonal line segments due to this mechanism are related to the largest positive Lyapunov exponent of the chaotic system.

The formation of Patterns (ii) is because of false recurrences due to insufficient embedding. Note that X_{i+k} and X_{j-k} go in opposite directions: if one goes to the forward direction of motion, then the other goes backwards. Suppose (A1,B1) are close together as shown in Figs. 3(a,b), then this means that (A2,B2) keep close together for a while. Typically this cannot be true, as can be readily envisioned by monitoring the uniform motion of two points along a circle (see also Fig. 3(a)). However, if all the points are projected onto the x-axis (dashed line in Fig. 3), then this becomes possible, and the two mechanisms for the formation of Patterns (i) will apply to this case as well.

Patterns (iii), the blocks, are now easy to explain. It is due to staggering motions around the turning points, O1, O2, O3, and O4, as shown in Fig. 3. Quite a bit portion of the orbits around those turning points, when projected onto the x-axis, are all close to those turning points. The forward motion then

gives the part of the blocks along the main diagonal, while the backward motion gives the part along the 135° diagonal. It should now be clear that the size of a block is proportional to the time that a trajectory stays close to a turning point in a 1-D embedding. If the motion of the system is quite uniform, then the blocks will be more or less of similar size (Figs. 2(A,C)). If the motion is not uniform, then the blocks may display quite different sizes (Fig. 2(E)). Since the speed of motion along an orbit also depends on the delay time L, we then see that RPs generally also depend on L. A good embedding would correspond to a more uniform and regular RP.

The above discussion should make it clear that when the data set is small, most of the false recurrences will be gone if the embedding dimension reaches 2. This can be clearly seen from Figs. 2(B1,D1,F1). However, some false recurrences around some points with very slow phase velocity may persist even when $m = 2$. This is indeed the case, as can be seen from Fig. 2(F1). Higher embedding ($m = 3$) further removes some of the remaining false recurrences (Fig. 2(F2)).

We are now at a good standing to review the statistics for RPs introduced in [3;14], and to understand how each statistic depends on the embedding parameters. There are five statistics: (i) the percentage of recurrent points, REC; (ii) the percentage of determinism, DET, which measures the percentage of recurrent points forming line segments which parallel the main diagonal (when the length of the lines exceed certain threshold); (iii) the Shannon entropy, ENT, of the distribution of those line segments which parallel the main diagonal; (iv) DIV, the inverse of the longest line segment which parallels the main diagonal; and (v) TREND, measures the 'paling' of the patterns of RP away from the main diagonal (used to detect drift and nonstationarity in a time series). Note that REC is simply what is used to compute the correlation dimension of a data set. Thus it is trivial to observe that this statistic sensitively depends on the embedding parameters. This is still true when this statistic is used to the study of a bifurcation sequence, as can been seen from Fig. 7 of Iwanski and Bradley [15]. We surmise that what Iwanski and Brandley really mean by embedding need not be done does not include this statistic. What is remarkable is that three statistics

are related to the patterns along the main diagonal. The most interesting result of [15] is that when these statistics are used to detect a bifurcation sequence (with carefully chosen threshold for the length of the lines), 1-D embedding has indeed already given a very good identification of the bifurcation sequence. How can this puzzling result be true?

It is indeed true. The reason is really quite simple. All these statistics belong to what we have classified as Patterns (i). The definitions of these statistics have automatically filtered out most of the false recurrences, as the latter belong to Patterns (ii). Hence, in a sense, these statistics are computed in an almost 2-D embedding. What we mean by almost is that some consequence of 1-D embedding is still there. That is, half of the Patterns (iii) (i.e., blocks) are still there, and sensitively depend on the embedding parameters (through the dependence of phase velocities on the latter). When the data is noisy, then the influence of these remaining structures will be larger, thus, embedding to a higher dimension will typically give better results. This issue will be further discussed in Section 5.

Before ending this section, we note an interesting feature reported by Iwanski and Bradley [15]. That is, the statistics (ii)-(-iv) sensitively depend on the threshold for the length of the lines. We shall explain the underlying mechanism for this in the next section.

3. Distribution of diagonal line segments for chaotic systems

It is remarkable that three of the five statistics proposed in [3;14], namely, DET, ENT, and DIV, are related to the line segments which parallel the main diagonal. To have a deeper understanding of those statistics, we consider the distribution of those line segments for chaotic systems. Note that by considering simple chaotic maps and assuming the delay time L to be 1, Faure and Korn [27] found the diagonal line segments to be exponentially distributed with K_2 entropy [28] as the only parameter,

$$P(k\delta t \leq t) = 1 - e^{-K_2 t} \tag{2}$$

where the integer k describes the length of the line segments, and δt is the sampling time, which is 1 for maps. We shall present a different argument to obtain a similar result. Our argument is based on a dynamical evolution point of view, and the result holds for arbitrary L.

Consider a diagonal line segment of length k, $k > 1$. That is, $\|X_{i+l} - X_{j+l}\| \leq d$, $l = 0, \ldots, k$, and $\|X_{i+k+1} - X_{j+k+1}\| > d$, where d is a prescribed small distance. Let $d_0 = \|X_i - X_j\|$. On average, we can write $d = d_0 e^{\lambda_o k \delta t}$, or in logarithmic scale, we have

$$\lambda_o k \delta t = \ln d - \ln d_0 \tag{3}$$

where λ_o is related but not identical to λ_1, the largest positive Lyapunov exponent (this will be further explained later). For chaotic signals, typically we can assume d_0 to follow a power law distribution,

$$P(d_0 \leq d) \sim d^{D_1} \tag{4}$$

Note, D_1 is not the correlation dimension, but the partial dimension corresponding to the most unstable direction, and typically assumes a value of 1 [29]. From Eqs. (3), (4), we can readily get the distribution for $k\delta t$,

$$P(k\delta t \leq t) = 1 - e^{-D_1 \lambda_o t} \tag{5}$$

Note that Eq. (5) expresses the cumulative probability distribution. The probability density function (pdf) is simply its derivative,

$$p(k\delta t) = D_1 \lambda_o e^{-D_1 \lambda_o t}. \tag{6}$$

It is an easy task to find that the mean and standard deviation of $k\delta t$ are both $1/(D_1 \lambda_o)$.

To verify Eq. (6), we estimate the pdf from the Henon map [30], $x(n + 1) = 1 + y(n) - 1.4x(n)^2$, $y(n + 1) = 0.3x(n)$; the chaotic Lorenz attractor (Eq. (1)); and the Mackey–Glass system [31], $\dot{x} = 0.2x(t + \Gamma)/(1 + x(t + \Gamma)^{10}) - 0.1x(t)$, with $\Gamma = 30$. The latter system has two positive Lyapunov expo-

nents [32]. Fig. 4 shows the estimated pdf's for these systems. Clearly we observe that the pdf's are exponentially distributed. The slopes of these curves are 0.32, 1.21, and 0.0067, for Henon, Lorenz, and Mackey–Glass systems, respectively. If we assume $D_1 = 1$, then these are the values for λ_o. Comparing with the values for λ_1, which are 0.42, 1.37, and 0.0071 [32], for Henon, Lorenz, and Mackey–Glass systems, respectively, we see that typically λ_o is a lower bound of λ_1. The reason is quite obvious. Accurate estimation of λ_1 should take both the diagonal line segments and the evolution of scattered pairs of recurring points into account [18–20]. Comparing Eq. (2) with Eq. (5), we find that $K_2 = D_1 \lambda_o$. Indeed, the obtained λ_o for the Henon map is very close to K_2 of [28] (but slightly smaller than that of [27]). This suggests that K_2 is not only a lower bound for the Kolmogorov entropy, which is the sum of the positive Lyapunov exponents [28], but also a lower bound for λ_1.

We can now understand DET, ENT and DIV better. The fundamental difference between REC and DET lies in the fact that the exponent D_1 governing the scaling law of Eq. (4) is 1 for DET (corresponding to the most unstable direction of the motion), while it is simply the correlation dimension for REC.
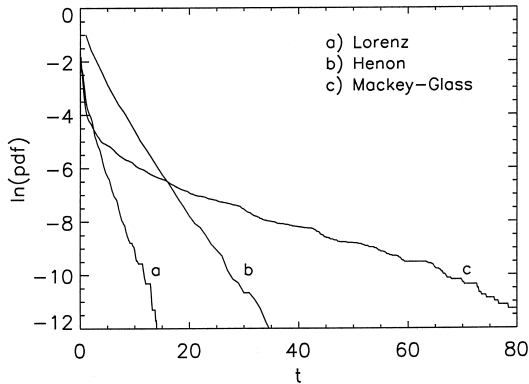

Fig. 4. Probability density function (pdf) in logarithmic scale versus time t. The parameters used are: $m = 2$, $L = 1$, $n = 5K$, $d = 2^{-4}$, for the Henon system; $m = 4$, $L = 3$, $n = 8K$, $d = 2^{-4}$, $\delta t = 0.06$, for the Lorenz system; and $m = 4$, $L = 6$, $n = 8K$, $d = 2^{-3}$, $\delta t = 1.5$, for the Mackey–Glass system with $\Gamma = 30$, where n is the total number of points. Note the units for t is 0.5 for the Lorenz system, 1 for the Henon map, and 10 for the Mackey–Glass system.

Now using the definition for the Shannon Entropy ENT [33],

$$\text{ENT} = \int_0^\infty p(t) \ln p(t) \, dt, \qquad (7)$$

we can easily find the associated ENT for the pdf of Eq. (6),

$$\text{ENT} = \ln(D_1 \lambda_o) - 1. \qquad (8)$$

When the Lyapunov exponent only slowly varies with the changes of dynamics, ENT would be an insensitive indicator of those changes.

Now we consider DIV. Recall the mean and standard deviation of $k \delta t$ are both $1/(D_1 \lambda_o)$. Hence, the longest diagonal line segment will roughly be twice as long as the mean of k, or,

$$\text{DIV} \approx \frac{D_1 \lambda_o \delta t}{2}. \qquad (9)$$

We thus see that this statistic has a more direct relation with the Lyapunov exponent.

While DET, ENT and DIV are quite simple statistics for characterizing the diagonal line segments, mean and standard deviation of those line segments give an even simpler characterization. For chaotic systems, it is the latter two that are truly reciprocals of the Lyapunov exponent.

In writing Eq. (3), we have assumed that X_i and X_j have been aligned along the unstable manifold of X_i or X_j. Typically this alignment needs time. Hence, too short diagonal line segments may not follow an exponential distribution. Observing Fig. 4 again, we indeed see that for small t, the distribution is not exponential (especially for the Mackey–Glass system). It is this re-adjustment time that provides an objective criterion for the selection of the threshold for the diagonal line segments. In other words, when the threshold is chosen at least as large as the re-adjustment time, then one would not observe the dependence of DET, ENT and DIV on the threshold, as reported by Iwanski and Bradley [15].

We mentioned that the concept of shell makes the interpretation and computation of certain statistics harder. Now we can see why this is so. On average, we can say that the divergence between X_i and X_j is

exponential. However, $\|X_{i+k} - X_{j+k}\|$, for positive k's, may not monotonically increase with the evolution time k. Sometimes it can actually shrink, while other times it can temporally fly apart. Either situation may induce the pair of points to escape a specific shell, thus breaks a continuous diagonal line segment. For this reason, we would not strongly suggest to use shells instead of balls for the construction of RPs, even though shells are more beneficial in the study of noisy time series.

Fig. 5. A schematic showing the recurrence points of the second type (solid circles) and the sojourn points (open circles) in $B_d(X_0)$.

4. Classification of recurrence points and detection of changes in dynamics

Recurrence points can be further divided into two classes [34]. This classification defines two types of recurrence times, hence, enables us to design new ways of quantifying a RP and detecting nonstationarity.

Let us arbitrarily choose a reference point X_l on the reconstructed trajectory, $\{X_i, i = 1,2, \cdots, N\}$, and consider recurrences to its neighborhood of radius d: $B_d(X_l) = \{X : \|X - X_l\| \leq d\}$. Denote the subset of the trajectory that belongs to $B_d(X_l)$ by $S_1 = \{X_{t_1}, X_{t_2}, \ldots, X_{t_i}\ldots\}$. These are the Poincaré recurrence points. When the ball $(0,d)$ is used to define a RP, then dots will be placed at points (l, t_i), $i = 1,2, \cdots$. From set S_1, we can define the Poincaré recurrence times by $\{T_1(i) = t_{i+1} - t_i, i = 1,2,\ldots\}$. For later convenience, we call $\{T_1(i)\}$ the recurrence times of the first type.

Sometimes we may have $T_1(i) = 1$ (for continuous time systems, this means 1 unit of sampling time), for some i. This corresponds to both X_{t_i} and $X_{t_{i+1}}$ belonging to S_1. For continuous time systems with fixed (small) sampling time, if the radius d of $B_d(X_l)$ is not too small, then we can have a sequence such as $X_{t_i}, X_{t_{i+1}}, \ldots, X_{t_{i+k}}$ belonging to S_1, with k on the order of 10 or even larger. This is schematically shown in Fig. 5. We call the sequence $X_{t_i+1}, \ldots, X_{t_i+k}$ (excluding X_{t_i}) sojourn points. When k is on the order of 10, each such sequence of points effectively represents a 1-D set. For maps or continuous time systems with small d, sojourn points are negligible, and form a 0-D (empty or almost empty) set. Now remove these points from S_1 and denote the
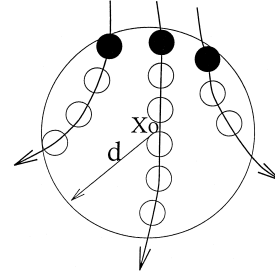
remaining points of S_1 by $S_2 = \{X_{t'_1}, X_{t'_2}, \ldots, X_{t'_i}\ldots\}$, which defines a time sequence $\{T_2(i) = t'_{i+1} - t'_i, i = 1,2,\ldots\}$. We call S_2 recurrence points of the second type, and $T_2(i)$ the recurrence times of the second type. For chaotic systems, we have shown [34] that the distributions of $\{T_2(i)\}$ is exponential, and the mean of $T_1(i)$ and $T_2(i)$ are both related to the information dimension of the attractor by simple scaling laws. For a periodic signal, $T_2(i)$ simply gives an estimation of the periodicity of the signal.

Note that the sojourn points trace out a vertical (by symmetry, also horizontal) line segment in a RP. It is these sojourn points that give the lines in Fig. 2 certain thickness, and make the structures of RPs wavy (especially for $m = 1$). Usually collection of sojourn points gives rise to square-like textures in RPs. Such square-like textures can be found in some dynamical systems [35;36]. More interesting, such textures are actually typical features of RPs constructed from biological data [2–13]. The underlying reason for the abundance of square-like textures in biological data may be because of the following two reasons: (i) in order that the data set is reasonably large, a quite high sampling frequency (i.e., a small sampling time) is usually used; (ii) in order that there are reasonably many points in a RP, a fairly large radius d will be typically adopted for constructing a RP.

Now we have a wealth of quantities to characterize a RP. Aside from the usual recurrence points, we also have the recurrence points of the second type, sojourn points, and two types of recurrence times. While sojourn points and the recurrence time of the

first type are not too useful for the study of a stationary chaotic system [34], they can also be very useful in detecting nonstationarity and changes of dynamics. Foe example, if one partitions a long time series into (overlapping or non-overlapping) blocks of data sets of short length, and computes RPs for each data set, one may observe that the square-like textures vary from block to block. This thus gives a convenient way of detecting some changes in dynamics.

Sojourn points give a different way to quantify certain deterministic features of a RP than the DET statistic, since the latter is for characterizing the diagonal line segments.

A possible third way to characterize certain other deterministic features of a RP is to use the afore mentioned tangential motion (its average effect gives the autocorrelation). This tangential motion is considered very unpleasant in the computation of the correlation dimension [26] and the Lyapunov exponents [18–20]. Nevertheless, it may be very useful and convenient in the study of changes in dynamics. Tangential motion also gives main diagonal line segments, as discussed earlier, and corresponds to a Lyapunov exponent of zero magnitude [37]. To obtain main diagonal line segments corresponding to the tangential motion, one needs only to do what is recommended not to do in [18–20;26], i.e., one simply tries to construct a truncated RP with a constraint: $1 \le |i - j| < w$, where w is a suitable integer, on the order of the period of one round orbital motion.

Before we end this section, we briefly discuss what the statistic TREND means. TREND is really an idea rather than a quantity. The feature that certain structure in a RP pales away from the main diagonal can be made more concrete by properly indexing the sojourn points and the recurrence times of the second type [34]. Also to detect certain changes in dynamics, one does not have to consider certain feature paling away from the main diagonal. Changes also manifest themselves along the main diagonal. After realizing this, then one can choose any quantity identified above and discussed in Section 4 to study the changes in dynamics such as a bifurcation sequence. Of course, depending on the concrete system one is studying, some quantities may reveal more information than other quantities. In the next section, we illustrate how to use the recurrence time of the second type to identify the bifurcation sequence of the noisy transient Lorenz system.

5. Case study: detection of bifurcations in the noisy transient Lorenz system

Following Iwanski and Bradley. [15], we consider a signal generated from the transient Lorenz system. The signal is generated from the Lorenz system (Eq. (1)), with a fourth-order Runge–Kutta method and a timestep of 0.01, by incrementing the parameter r from 28.0 to 268.0 by 0.002 at each integration step. The signal, of total length 120001, is shown simply by dots in Fig. 6(a). Theoretically, there are three periodic windows: $99.524 < r < 100.795$, $145 < r < 166$, and $r > 214.4$, as indicated by dashed vertical lines in Fig. 6(a). However, we shall emphasize that the whole data set is really a transient signal. It is due to this transient nature of the signal that we do not really see a distinct transition near the parameter value around 214.4. In other words, the signals corresponding to some small interval of $r < 214.4$ look similar to those corresponding to $r > 214.4$. We shall also note that three small segments of the signal, which are right below the capital letters A, B, and C, as indicated in Fig. 6(a), look strange. Do those segments of the signal correspond to some periodic motion with very distinct periods? Careful examination of those segments just reveals that there is really no strangeness about those segments at all. The visual effect is simply due to sampling: it just so happens that the signal $x(t)$ more or less takes on a discrete set of values in those parameter intervals (recall that Fig. 6(a) is plotted as dots. If they are connected by lines, then this strangeness is gone). To have a better feeling about what the signals look like, we have also shown in Figs. 6(b,d) two small segments of the signal (1000 and 500 points, respectively), and in Figs. 6(c,e) their corresponding phase diagrams. Note the 'attractor' in Fig. 6(c) looks like the usual Lorenz attractor. We note from Fig. 6(d) that the segment of the time series contains approximately 10 waves. Hence, the 'periodicity' is roughly 50 sampling points. However, Fig. 6(e) reminds us of a period-doubled limit cycle, hence, in a finer resolution, the periodicity should be around 100 sampling points.

Fig. 6. (a) The transient Lorenz signal; (b,d) portions of the signal; and (c,e) their corresponding phase diagrams.

We choose the recurrence time of the second type to study this signal. As before, we first normalize the whole time series into the unit interval, (0,1). We then compute $\overline{T}_2(r)$ on time series data within episodic windows consisting of 1000 consecutive points. Sequential windows are shifted by 10 points (thus overlapping by 990 points), giving a total of 11901 values for $\overline{T}_2(r)$.

First, we consider the clean signal. Figs. 7(a–d) show $\overline{T}_2(r)$ versus the parameter r for different embedding dimensions and scales d. The three theoretically known periodic windows are roughly indi-
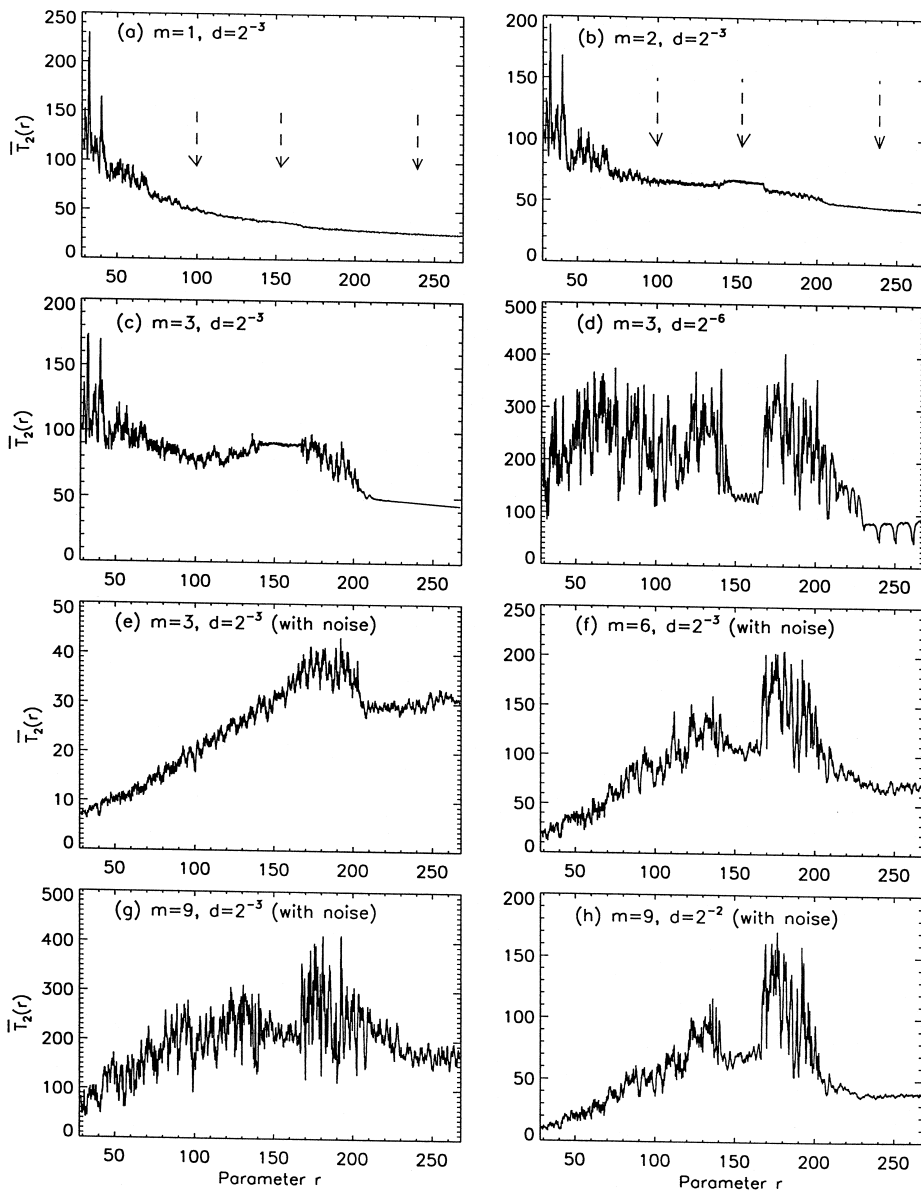
Fig. 7. Variation of $\bar{T}_2(r)$ with the parameter r. The delay time L is always 10. See the text for other details.

cated by three dashed arrows. We observe that $m = 1$ (Fig. 7(a)) does not give any indication of a bifurcation sequence, though it does indicate that the time series is nonstationary ($\bar{T}_2(r)$ would be more or less a constant for a stationary signal). The basic feature of the curve for $m = 1$ persists even when different scales d are used. The curve with $m = 2$ (Fig. 7(b)) gives a much better result, as it indeed correctly

locates the two large periodic windows. It even captures the rough scale 'periodicity' of the signal (about 50 sampling points, Fig. 6(d)). The first small periodic window is actually also identified, if one blows up that portion of the curve. However, the changes in the chaotic regions has not been clearly indicated. Hence, overall, we shall consider that $m = 2$ is still too small. Indeed, the curve for $m = 3$

(Fig. 7(c)) is a lot better. It correctly indicates everything: chaotic and periodic regions, the rough-scale periodicity for the periodic windows, and wild changes inside the chaotic regions. If we use a smaller scale to compute $\bar{T}_2(r)$, then we obtain Fig. 7(d). While the basic features of Fig. 7(d) is similar to those of Fig. 7(c), we do see some differences, especially inside the third periodic window. In that parameter region, most of the $\bar{T}_2(r)$ is around 100, corresponding to what we have observed from Fig. 6(e). However, we also observe three large dips. Note those dips also show up in Fig. 7 of Iwanski et al. [15]. Do they indicate fine bifurcations inside that periodic window?

The answer is no. It is due to the fact that around those specific small parameter intervals, the amplitude of the signal hardly changes, giving a simple limit cycle, as compared to the period-doubled limit cycle of Fig. 6(e).

Next we add Gaussian white noise to the signal. The amplitude of the noise is about $1/3$ of that of the signal, giving an SNR of 10 dB (i.e., the variance of the noise is 0.1 of that of the signal). Note this noise is really quite large. We shall also note that the amplitudes of the signals for small parameter values of r are much smaller than those for large r values, hence, those parts of the signals really have a higher noise level.

Figs. 7(e–h) show $\bar{T}_2(r)$ versus the parameter r for different embedding dimensions and scales d for the noisy signal. First we observe that the signals corresponding to smaller parameter values of r are affected more by the noise. Next we observe that the pleasing result of Fig. 7(c) is now gone: only the third periodic window is roughly identified with $m = 3$ (Fig. 7(e)). This should be understandable. A noisy signal is really infinite-dimensional. This suggests us to use a larger embedding dimension. Indeed, with $m = 6$ (Fig. 7(f)), we recover most of the nice features of Fig. 7(c). Will the result be even better with an even larger m? The answer is both yes and no. With most of the scales we tried, the result is actually worse, as can be seen by comparing between Fig. 7(g) and (f). This can be understood if one realizes that in a higher dimension, the effects of noise would be stronger. This suggests that using a larger scale d, one might be able to re-obtain, or even improve the result of Fig. 7(f). This is indeed

so, as is shown in Fig. 7(h). The improvement of Fig. 7(h) over Fig. 7(f) lies in the fact that the periodicity for the third periodic window is more close to 50 in Fig. 7(h). However, we should emphasize that the good scales of d becomes much narrower and more difficult to find for very large embedding dimensions. Hence, we would suggest that one stop at some reasonably large embedding dimensions such as $m = 6$, since anyway, the data set used to compute $\bar{T}_2(r)$ (or other statistics) is quite small (1000 points here).

6. Conclusions

We have carefully studied the structures of a RP, especially when the embedding dimension is 1. We have identified four basic patterns of a RP, and studied the mechanisms for the generation of those patterns. These considerations enable us to understand how the structures of and quantification statistics for RPs vary with the embedding parameters. In particular, these considerations have demystified the paradoxical results of Iwanski and Bradley [15]. By considering the distribution of the main diagonal line segments for chaotic systems, we relate some of the known statistics for the quantification of a RP to the Lyapunov exponent. This consideration enables us to introduce new statistics to quantify the diagonal line segments. Those new statistics have a more direct relation with the Lyapunov exponent. Furthermore, we categorize recurrence points into two classes. This classification enables us to identify a number of new quantities which may be useful for the detection of nonstationarity in a time series, especially for the detection of a bifurcation sequence. A noisy transient Lorenz system is studied, to demonstrate how to identify a true bifurcation sequence, to interpret false bifurcation points, and to choose the embedding dimension.

References

[1] J.P. Eckmann, S.O. Kamphorst, D. Ruelle, Europhys. Lett. 4 (1987) 973.

[2] P. Kaluzny, R. Tarnecki, Biol. Cybern. 68 (1993) 527.

[3] C.L. Webber, J.P. Zbilut, J. Appl. Physiol. 76 (1994) 965.

[4] C.L. Webber, M.A. Schmidt, J.M. Walsh, J. Appl. Physiol. 78 (1995) 814.

[5] J.P. Segundo, M. Stiber, J.F. Vibert, S. Hanneton, Neurosci. 68 (1995) 657.

[6] A. Gottschalk, M.S. Bauer, P.C. Whybrow, Arch. General Psych. 52 (1995) 947.

[7] P. Faure, H. Korn, Proc. Nat. Acad. Sci. USA 94 (1997) 6506.

[8] J.P.M. Pijn, D.N. Velis, M.J. vanderHeyden, J. DeGoede, C.W.M. vanVeelen, F.H.L. daSilva, Brain Topogr. 9 (1997) 249.

[9] M. Shelhamer, J. Neurosci. Methods 83 (1998) 45.

[10] A. Giuliani, G. Piccirillo, V. Marigliano, A. Colosimo, Am. J. Physiol. 275 (1998) 1455, H.

[11] J.P. Zbilut, A. Giuliani, C.L. Webber, A. Colosimo, Protein Eng. 11 (1998) 87.

[12] A. Giuliani, R. Benigni, P. Sirabella, J.P. Zbilut, A. Colosimo, Biophys. J 78 (2000) 136.

[13] C. Manetti, M.A. Ceruso, A. Giuliani, C.L. Webber, J.P. Zbilut, Phys. Rev. E 59 (1999) 992.

[14] L.L. Trulla, A. Giuliant, J.P. Zbilut, C.L. Webber, Phys. Lett. A 223 (1996) 255.

[15] J.S. Iwanski, E. Bradley, Chaos 8 (1998) 861.

[16] N.H. Packard, J.P. Crutchfield, J.D. Farmer, R.S. Shaw, Phys. Rev. Lett. 45 (1980) 712.

[17] F. Takens, in: D.A. Rand, L.S. Young (Eds.), Dynamical Systems and Turbulence, Lecture Notes in Mathematics, vol. 898, Springer, Berlin, 1981, p. 366.

[18] J.B. Gao, Z.M. Zheng, Phys. Lett. A 181 (1993) 153.

[19] J.B. Gao, Z.M. Zheng, Europhys. Lett. 25 (1994) 485.

[20] J.B. Gao, Z.M. Zheng, Phys. Rev. E 49 (1994) 3807.

[21] J.B. Gao, Phys. Rev. Lett. 82 (1999) 1132.

[22] J.B. Gao, Physica D 78 (1997) 220.

[23] J.B. Gao, C.C. Chen, S.K. Hwang, J.M. Liu, Int. J. Mod. Phys. B 13 (1999) 3283.

[24] J.B. Gao, S.K. Hwang, J.M. Liu, Phys. Rev. A 59 (1999) 1582.

[25] E.N. Lorenz, J. Atmos. Sci. 20 (1963) 130.

[26] J. Theiler, Phys. Rev. A 34 (1986) 2427.

[27] P. Faure, H. Korn, Physica D 122 (1998) 265.

[28] P. Grassberger, P. Procaccia, Phys. Rev. A 28 (1983) 2591.

[29] P. Grassberger, in: A.V. Holden (Ed.), Chaos, Princeton, New Jersey, 1986, pp. 294.

[30] M. Henon, Commun. Math. Phys. 50 (1976) 69.

[31] M. Mackey, L. Glass, Science 197 (1977) 287.

[32] M. Sano, Y. Sawada, Phys. Rev. Lett. 55 (1985) 1082.

[33] T.M. Cover, J.A. Thomas, Elements of information theory, Wiley, New York, 1991.

[34] J.B. Gao, Phys. Rev. Lett. 83 (1999) 3178.

[35] M.C. Casdagli, Phys. D 108 (1998) 12.

[36] J.P. Zbilut, A. Giuliant, C.L. Webber, Phys. Lett. A 237 (1998) 131.

[37] H. Haken, Phys. Lett. A 94 (1983) 71.